Structural, Magnetic, and Transport Properties of the Two Electron-Doped Ruddlesden–Popper Manganites $Ca_{3-x}Th_xMn_2O_7$

Maxim V. Lobanov, Siwen Li, and Martha Greenblatt*

Department of Chemistry and Chemical Biology, Rutgers, The State University of New Jersey, Piscataway, New Jersey 08854

Received October 2, 2002. Revised Manuscript Received January 6, 2003

New $Ca_{3-x}Th_xMn_2O_7$ ($x = 0$–0.2) compounds with the Ruddlesden–Popper structure have been synthesized. Their crystal structures were refined from X-ray powder diffraction data, taking into account a small orthorhombic (space group *Cmcm* or *Cmc*2_1) distortion of the parent tetragonal $I4/mmm$ structure. Doping of $Ca_3Mn_2O_7$ with tetravalent Th produces a significant ferromagnetic (FM) component in the magnetization at $x = 0.05$, which diminishes with a further increase of x and completely disappears at $x = 0.2$. This behavior is compared with single-electron La doping and shows universal scaling of magnetic properties with electron concentration as observed for three-dimensional perovskites as well. A model for the magnetic structure evolution has been proposed on the basis of symmetry conditions for weak ferromagnetism and the structural changes observed. A large negative magnetoresistance (MR) was observed with a maximal value of -66% for the $x = 0.05$ composition. The temperature and field dependence of MR suggests its tunneling origin. The MR and the weak ferromagnetic component disappear simultaneously at $x = 0.2$, and a two-dimensional variable range hopping conduction due to confinement of charge carriers within perovskite bilayers is observed.

Introduction

Complex manganese oxides have been a subject of remarkable interest in recent years due to the colossal magnetoresistance (CMR) effect.[1] The technological application of the three-dimensional (3D) perovskites $Ln_{1-x}A_xMnO_3$ (Ln = lanthanide, A = Sr, Ca) is precluded by the high driving magnetic field necessary to produce the desired resistivity drop. Layered compounds can provide an efficient mechanism of intrinsic low-field magnetoresistance due to interplane tunneling. This effect was first observed in the so-called Ruddlesden–Popper (RP) compound $La_{1.4}Sr_{1.6}Mn_2O_7$.[2] The crystal structure of RP phases $(AO)(ABO_3)_n$ consists of perovskite blocks (*n* layers of ABO_3) separated by a rock-salt (AO) intermediary. For $n = 2$ the perovskite fragment is commonly referred to as "bilayer".

The RP phases typically show complex evolution of magnetic and transport properties as a function of composition, generally paralleling the corresponding 3D (perovskite) compounds $Ln_{1-x}A_xMnO_3$. The latter are known to exhibit CMR both in the "hole-doped" ($x < 1/2$) and "electron-doped" ($x > 1/2$) regimes. Especially, the $n = 1$ RP manganites exhibit CMR only in the electron-doped regime in a narrow doping range.[3] The $Ca_{n+1}Mn_nO_{3n+1}$ ($n = 1$–3, ∞) RP compounds have been first synthesized by MacChesney et al.[4] and reinvestigated recently by Fawcett et al.[5] All these compounds are antiferromagnets (AF) with Néel temperatures in the 110–130 K range. For all nonperovskite ($n \neq \infty$) phases the high-temperature susceptibility deviates significantly from the Curie–Weiss law and suggests two-dimensional (2D) magnetism. Detailed magnetic study of the $n = 3$ compound showed complicated field-dependent magnetic behavior.[6]

Two-electron doping (with tetravalent Ce or Th ions) usually produces the evolution of properties resembling the corresponding single-electron doping. Considering the $Ln_{1-x}Ca_xMnO_3$ system in the electron-doped regime, with the increase of Ln content there is a gradual increase of the ferromagnetic component within the canted antiferromagnetic (CAF) structure up to some critical *x* value, followed by the onset of charge ordering (CO) visible as a peak in the magnetization curves. The *x* value is approximately twice as small for tetravalent Ce and Th compared to that for trivalent lanthanides, consistent with the expected twice as high electron concentration for the same x.[7]

Single-electron-doped compounds $Ca_{3-x}La_xMn_2O_7$ were investigated in ref 8. Single-phase compositions have been synthesized in a broad composition range. The

* Corresponding author. E-mail: martha@rutchem.rutgers.edu. Fax: 011-732-445-5312.

(1) See for example Salamon, M. B.; Jaime, M. *Rev. Mod. Phys.* **2001**, *73*, 583.

(2) Kimura, T.; Tomioka, Y.; Kuwahara, H.; Asamitsu, A.; Tamura, M.; Tokura, Y. *Science* **1996**, *274*, 1698.

(3) Maignan, A.; Martin, C.; Van Tendeloo, G.; Herview, M.; Raveau, B. *J. Mater. Chem.* **1998**, *8*, 2411.

(4) MacChesney, J. B.; Williams, H. J.; Potter, J. F.; Sherwood, R. C. *Phys. Rev.* **1967**, *164*, 779.

(5) Fawcett, I. D.; Sunstrom, J. E.; Greenblatt, M.; Croft, M.; Ramanujachary, K. V. *Chem. Mater.* **1998**, *10*, 3643.

(6) Lago, J.; Battle, P. D.; Rosseinsky, M. J. *J. Phys. C* **2000**, *12*, 2505.

(7) Maignan, A.; Martin, C.; Damay, F.; Raveau, B. *Chem. Mater.* **1998**, *10*, 950.

evolution of magnetic properties resembles that of corresponding electron-doped perovskites. The CAF structure is stable up to $x = 0.3$, whereas the CO state is realized above $x = 0.4$. The "crossover" $x = 0.35$ composition shows complicated magnetic behavior.

Experimental Section

The single-phase $Ca_{3-x}Th_xMn_2O_{7-\delta}$ ($x = 0-0.2$) compounds have been prepared by the citrate sol−gel technique. Stoichiometric amounts of $CaCO_3$ (Aldrich, 99+%, preheated at 300 °C), $Th(NO_3)_4 \cdot xH_2O$ ($x = 4.67$, as determined by TGA) and $Mn(NO_3)_2$ (Aldrich, 49.7 wt % solution in nitric acid) were dissolved in dilute (~ 2 M) nitric acid; then, an excess of citric acid and ethylene glycol was added. After all the reactants had dissolved, the solution was heated on a hot plate, resulting in the formation of a gel. The gel was dried at 300 °C and then heated at 600 °C overnight to remove the organic compounds and decompose the nitrates. The resultant powder was pressed into pellets and fired at 1300 °C for 4 weeks in air, with multiple intermediate regrindings. After annealings the samples were quenched to room temperature. Samples with $x > 0.2$ cannot be synthesized as single phases by this technique.

Powder X-ray diffraction (PXD) data for Rietveld analysis were obtained with either a Scintag PAD V (Cu Kα radiation, Ge solid-state detector) or Bruker D8 Advance (Cu Kα radiation, diffracted beam graphite monochromator, scintillation counter) diffractometers. Fullprof[9] and TOPAS[10] programs were used for Rietveld refinement and profile matching.

Magnetic measurements were performed with a Quantum Design SQUID magnetometer (MPMS-XL). Magnetoresistance measurements were performed on the same machine using External Device Control and Keithley equipment utilizing the standard four-probe technique.

Results and Discussion

Crystal Structure. Justification of Model. The X-ray diffraction patterns for all the compounds investigated can be indexed in an I-centered tetragonal cell with no systematic extinctions, consistent with the $I4/mmm$ model proposed previously for a variety of RP compounds. Profile matching (by Le Bail method) yielded unit cell parameters depending monotonically on the Th content up to $x = 0.2$.

However, complicated hkl-dependent peak broadening has been observed for all compositions. This feature can indicate small crystal structure distortions, which are typically too small in magnitude to provide clear reflection splitting. The magnetic susceptibility (see below) indicates the presence of a weak ferromagnetic (WFM) component below T_N. This is very typical and usually attributed to the Dzyaloshinskii−Moriya interaction (DM, antisymmetric exchange).[11,12] However, DM interaction vanishes by symmetry in a tetragonal $I4/mmm$ model.[13] Therefore, the orthorhombic structure distortion which would allow WFM component appears necessary, at least in the magnetically ordered state.
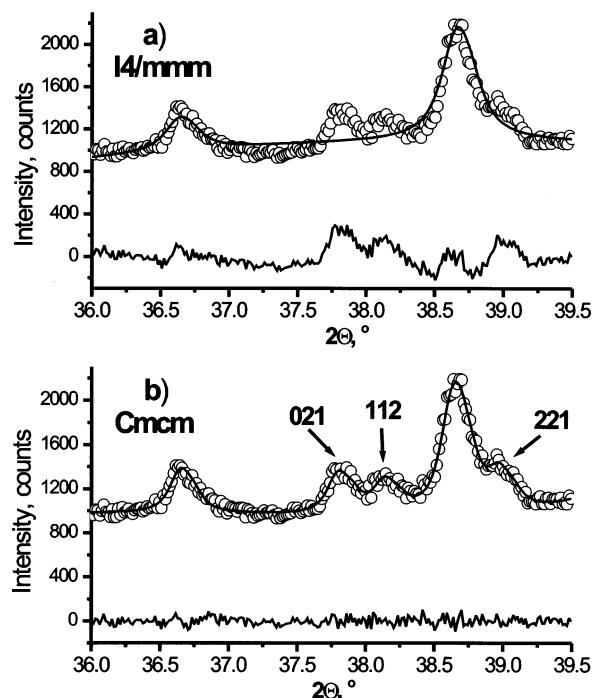

Figure 1. Fit (Le Bail) of the $36 < 2\theta < 39.5°$ region of the PXD spectrum of $Ca_{2.8}Th_{0.2}Mn_2O_7$ in (a) tetragonal ($I4/mmm$) and (b) orthorhombic ($Cmcm$) models. Miller indices for the observed superlattice reflections are shown.

Careful investigation of the diffraction profile revealed the presence of very weak reflections, which are forbidden by tetragonal symmetry. In Figure 1 a selected region of the PXD pattern for $x = 0.2$, scanned with 175 s/step, is shown. Superlattice reflections are clearly observed; they can be indexed as (021), (112), and (221) in a C-centered orthorhombic lattice with cell parameters $a_o \sim c_t$, $b_o \sim c_o \sim \sqrt{2}a_t$ (subscripts "o" and "t" refer to a new orthorhombic and parent tetragonal lattices, respectively).

In a recent investigation of $Ca_{3-x}La_xMn_2O_7$ ($x = 0-0.4$) by electron diffraction it was also claimed that the crystal structure at room temperature is orthorhombic with either $Cmc2_1$ or $Cmcm$ space symmetry.[14,15] The $Cmc2_1$ model was found to be the most likely on the basis of dark-field imaging observations. This model corresponds to a $(\Phi\Phi\Psi_z/\Phi\Phi\Psi_z)$ tilt system in the notation of Aleksandrov and Bartholome[16] (or $a^-a^-c^+/a^-a^-c^+$ in a more conventional Glazer one). The $Cmcm$ model corresponds to the $(\Phi\Phi 0/\Phi\Phi 0)$ system with no z-component of tilt. It was shown also that the observed structural transition from the high temperature $I4/mmm$ phase does not coincide with the onset of magnetic order. The $Cmcm$ structure has been found by neutron diffraction for $Ca_2LaMn_2O_7$.[17] However, unusually high and anisotropic thermal factors have been observed, which might indicate further symmetry lowering, for example, to $Cmc2_1$. The $Cmc2_1$ symmetry has been recently claimed for the undoped $Ca_3Mn_2O_7$ on the basis of a single-crystal X-ray study.[18]

(8) Fawcett, I. D.; Kim, E.; Greenblatt, M.; Croft, M.; Bendersky, L. A. *Phys. Rev.* **2000**, *B62*, 6485.

(9) Rodriguez-Carvajal, FULLPROF: A Program for Rietveld Refinement and Pattern Matching Analysis. In *Abstracts of the Satellite Meeting on Powder Diffraction of the XV Congress of the IUCr*, p 127 Toulouse, France (1990).

(10) Cheary, R. W.; Coelho, A. A. J. *Appl. Crystallogr.* **1992**, *25*, 109.

(11) Dzyaloshinskii, I. *J. Phys. Chem. Solids* **1958**, *4*, 241.

(12) Moriya, T. *Phys. Rev.* **1961**, *120*, 91.

(13) Turov, E. A. *Physical Properties of Magnetically Ordered Crystals*; Academic Press: New York, 1965; Chapter 5.

(14) Bendersky, L. A.; Chen, R.; Fawcett, I. D.; Greenblatt, M. J. *Solid State Chem.* **2001**, *157*, 309.

(15) Bendersky, L. A.; Greenblatt, M. Unpublished.

(16) Aleksandrov, K. S.; Bartholome, J. *J. Phys. C* **1994**, *6*, 8219.

(17) Green, M. A.; Neumann, D. A. *Chem. Mater.* **2000**, *12*, 90.

(18) Guiblin, N.; Grebille, D.; Leligny, H.; Martin, C. *Acta Crystallogr.* **2002**, *C58*, i3.

The initial profile-matching attempt has been performed first with Scintag data, which are characterized by a relatively low resolution. For these data analytical pseudo-Voigt profile function provides a reasonable fit. However, when this approach was attempted with the higher resolution Bruker data, this led often to unstable or divergent refinements. Therefore, a fundamental parameters approach,[10] implemented in the TOPAS software, has been used to model the peak shape. This approach is known to provide better refinement stability. The profile matching revealed significant preference of orthorhombic fit over the tetragonal one for all compositions; the values of reliability factors for $x = 0.20$, measured with the highest statistics (29 s/step), are $R_p = 7.01\%$, $R_{wp} = 9.29\%$ vs $R_p = 8.30\%$, $R_{wp} = 10.98\%$.

The two orthorhombic models (*Cmcm* and *Cmc2₁*) are virtually indistinguishable by laboratory X-ray diffraction. They are the same metrically (including extinction conditions), whereas additional tilt (Ψ_z) is beyond the detection of laboratory PXD. Therefore, Rietveld refinement has been undertaken in the more symmetric *Cmcm* model. The initial cation positions were taken from ref 12 (special positions in the *I4/mmm* model, transformed to the orthorhombic lattice). The oxygen positions were refined with "order parameters" Δ_x and Δ_y, constrained to yield the same tilt magnitude (ϕ) according to the relations;[12] "t" subscripts mean "tetragonal cell":

$$\Delta_x = \frac{\sqrt{2}a_t}{4c_t}\tan \phi \qquad (1)$$

$$\Delta_y = \frac{1}{2\sqrt{2}}\tan \phi \qquad (2)$$

This model yields reasonable values of reliability factors ($R_p = 9.64\%$, $R_{wp} = 12.76\%$, GOF = 2.13 for the $x = 0.20$ compound). The refinement also showed the presence of an A-site order. This can be concluded from a significant observed intensity ($I_{obs} = 1.9\%$) of (311/600)$_o$ doublet, which is otherwise nearly vanishing, and unphysical thermal factors for A-cations ($B_{4c} = -0.93$ Å², $B_{8g} = 2.58$ Å²), obtained assuming a completely disordered model. The direct refinement of relative occupancies failed; therefore, they have been estimated from the minimum of R_{wp} as a function of relative occupancy of the A-cation (4c) site by Ca (g_1) and simultaneously from the intercept of the dependencies of A-cations thermal factors on g_1 (Figure 2). The "true" value is expected to lie somewhere between these two boundaries (i.e., in the $0.85 \leq g_1 \leq 0.90$ range). These results indicate that Th preferentially occupies (4c) sites within the perovskite block. Similar cation redistribution has been found in Ca₂LaMn₂O₇ by neutron diffraction.[17] This model provides a nearly perfect description of the (311/600)$_o$ doublet as well. Atomic parameters for Ca₂.₈Th₀.₂Mn₂O₇ are summarized in Table 1; the fit of the entire diffraction spectrum is shown in Figure 3. The crystal structures for the compounds with other x values have been refined in the same model assuming identical distribution of Th between the two A-sites.

Crystal Structure. Evolution with Th Content.
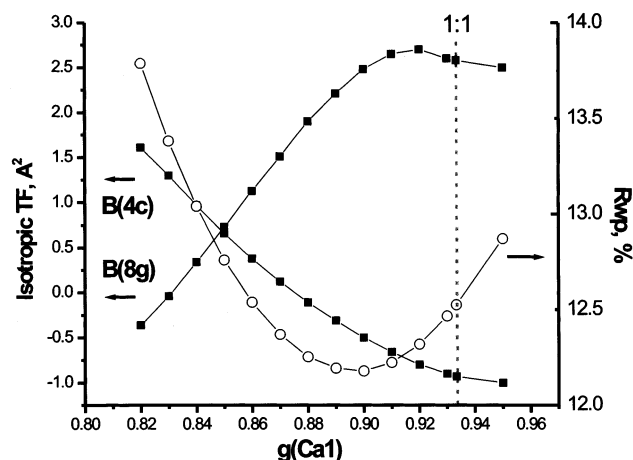The crystal structure of $n = 2$ Ruddlesden–Popper

Figure 2. Left axis: variation of isotropic thermal factors of two A-cation sites as a function of relative occupancy of the (4c) site by Ca (g_{Ca1}). Right axis: R_{wp} as a function of g_{Ca1}. Lines are guides to the eye. Vertical dashed line denotes "equidistribution" point (no A-site order).
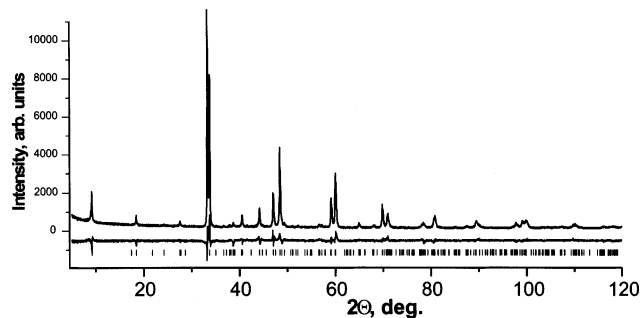

Figure 3. Experimental and difference PXD patterns for Ca₂.₈-Th₀.₂Mn₂O₇. Tick marks show theoretical positions of reflections.

Table 1. Atomic Parameters for the Ca₂.₈Th₀.₂Mn₂O₇ (space Group *Cmcm*, All Occupancies Are Fixed, Thermal Factors for Oxygen Atoms Are Refined as Common)

atom	site	occupancy	x	y	z	B, Å²
Ca/Th1	4c	0.85/0.15	¹/₂	0.743	³/₄	0.6
Ca/Th2	8g	0.975/0.025	0.312	0.731	³/₄	0.8
Mn	8g	1	0.101	0.750	³/₄	0.1
O1	4c	1	0	³/₄ − Δ_y	³/₄	3.0
O2	8e	1	0.101 − Δ_x	0	0	3.0
O3	8e	1	0.101 + Δ_x	¹/₂	0	3.0
O4	8g	1	0.203	³/₄ + Δ_y	³/₄	3.0

$\Delta_x = 0.0076(5)$, $\Delta_y = 0.039(2)$

phases is shown in Figure 4. The structure undergoes profound evolution with increasing Th substitution. The unit cell parameters, volumes, orthorhombic distortion parameter $\xi = |b - c|/(b + c)$ and octahedral tilt angle ϕ (from eq 2) are summarized in Table 2. The in-plane cell parameters (b and c) and cell volume increase monotonically with increasing x, consistent with the increasing Mn³⁺ fraction (ionic radii are Mn³⁺, CN = 6, high spin, 0.64 Å; Mn⁴⁺, CN = 6, 0.53 Å).[19] The tilt angle shows strong monotonic increase with increasing x; this naturally explains the observed reduction of the a (long axis) parameter.

The evolution of Mn–O interatomic distances and relevant bond angles as a function of Th content is

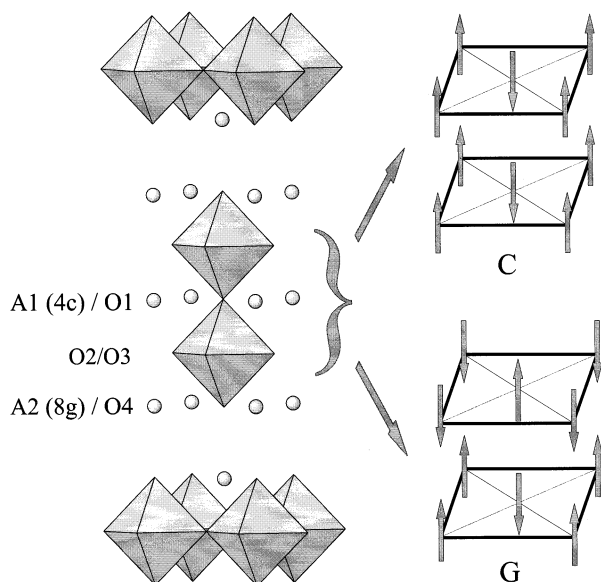(19) Shannon, R. D.; Prewitt, C. T. *Acta Crystallogr.* **1969**, *B25*, 925.

Figure 4. Left: Schematic representation of the crystal structure of $n = 2$ Ruddlesden−Popper phases. Two inequivalent A-sites and four oxygen positions are marked. Right: Schematic representation of the magnetic structures (for one bilayer), denoted as G- and C-type.

Table 2. Cell Parameters, Volumes, Orthorhombic Distortion Parameter $\xi = |b - c|/(b + c)$, and Octahedral Tilt Angle ϕ of $Ca_{3-x}Th_xMn_2O_7$ (Orthorhombic C-Centered Cell)

x	a, Å	b, Å	c, Å	V, Å^3	$\xi \times 10^4$	ϕ, deg
0	19.4365(8)	5.2461(3)	5.2411(3)	534.41(8)	4.8	1.0
0.05	19.3700(9)	5.2673(4)	5.2607(5)	536.74(12)	6.3	2.6
0.10	19.3562(7)	5.2869(3)	5.2792(3)	540.24(8)	7.3	4.4
0.15	19.3362(6)	5.3045(2)	5.2971(2)	543.32(6)	7.0	5.9
0.20	19.3151(6)	5.3196(2)	5.3111(2)	545.71(6)	8.0	6.3

Table 3. Interatomic Mn−O Distances, Relevant Bond Angles, and Octahedral (Jahn−Teller) Distortion σ for $Ca_{3-x}Th_xMn_2O_7$

x	Mn−O1, Å	Mn−O2, Å	Mn−O3, Å	Mn−O4, Å^3	∠(Mn−O1−Mn), deg	σ
0	1.921	2 × 1.870	2 × 1.844	1.793	172.6	0.022
0.05	1.979	2 × 1.876	2 × 1.854	2.035	176.1	0.040
0.10	1.971	2 × 1.876	2 × 1.868	1.993	171.7	0.030
0.15	1.971	2 × 1.885	2 × 1.874	1.954	168.9	0.023
0.20	1.966	2 × 1.886	2 × 1.884	1.972	167.9	0.023

presented in Table 3. The most remarkable structural feature is the evolution of the Mn−O1−Mn bond angle, which has profound implication on the magnetic data interpretation (see below). Unexpectedly, evolution of interatomic distances does not follow simple expectations based on the increase of Jahn−Teller ion (Mn^{3+}) concentration. In Table 3, values of the "Jahn−Teller distortion parameter"

$$\sigma = \sqrt{\frac{1}{6} \sum_i (r_i - \langle r \rangle)^2}$$

(r_i are observed Mn−O interatomic distances and $\langle r \rangle$ is the average one) are presented. It does not depend monotonically on the Th concentration. More precise structural study (e.g., with neutron diffraction) is necessary to clarify this subject. However, this effect can stem from the constrained refinement (see above).

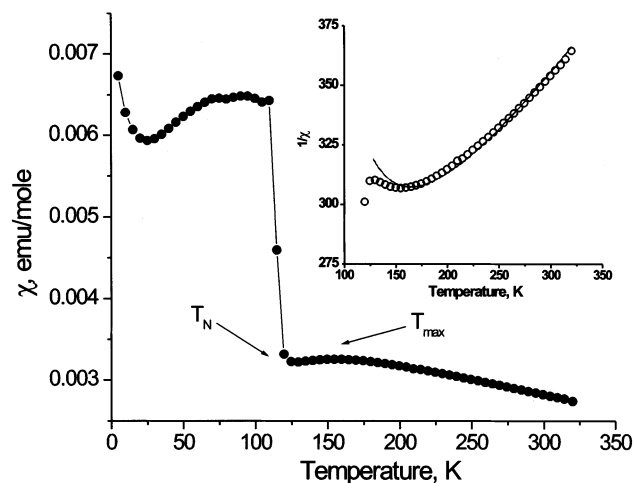**Magnetic Properties.** The temperature dependence of dc magnetic susceptibility, χ, for $Ca_3Mn_2O_7$ is shown

Figure 5. Temperature dependence of dc magnetic susceptibility of $Ca_3Mn_2O_7$ (external field $H = 100$ Oe). T_N denotes the Néel temperature, and T_{max} marks a 2D maximum. Inset: fit of the high-temperature inverse susceptibility to a series expansion for a 2D Heisenberg AF. Line is a best fit.

in Figure 5. A broad maximum, characteristic of low-dimensional magnetism, is visible at $T_{max} \sim 155$ K. The exchange integral J has been estimated using the expression[20] for the Heisenberg model on a square planar lattice for $S = 2$

$$k_B T_{max}/JS(S + 1) = 2.07 \tag{3}$$

as $J/k_B = -19.7$ K. A similar value of J is obtained using a 2D Ising model. An attempt of a quantitative analysis has been undertaken with the high-temperature series (HTS) expansion for a 2D Heisenberg antiferromagnet with six coefficients (C_n) from ref 21 ($\theta = k_B T/J$ is the reduced temperature):

$$Ng^2\mu_B^2/\chi J = 3\theta + \sum_{n=1}^{\infty} \frac{C_n}{\theta^{n-1}} \tag{4}$$

The HTS fit of the inverse susceptibility is shown in the inset of Figure 5. The fit yields $J/k_B = 41.5$ K and an unphysical value of $g = 3.3$. This result is identical to that obtained in ref 6 for $Ca_4Mn_3O_{10}$; the explanation proposed by Lago et al.[6] is that the pure 2D fit does not provide quantitatively a good description for RP compounds, where an effective magnetic dimensionality D is between 2 and 3. The field dependence of magnetization at 5 K reveals slight hysteresis and an absence of saturation up to 5 T applied field, consistent with a CAF state.

Th substitution has a profound effect on the magnetic properties. For $x \leq 0.15$ the system remains a CAF. The temperature dependence of χ is shown in Figure 6 a−c. The observed divergence between field-cooled (FC) and zero-field-cooled (ZFC) susceptibilities is typical for CAFs. The evolution of the FM component can be quantitatively monitored from low-temperature magnetization isotherms. For doped compounds ($x = 0.05, 0.10$) the analysis is straightforward.

(20) Navarro, R. In *Magnetic Properties of Layered Transition Metal Compounds*; de Jongh, L. J., Ed.; Kluwer Academic Publishers: Dordrecht, The Netherlands, 1990; p 105.
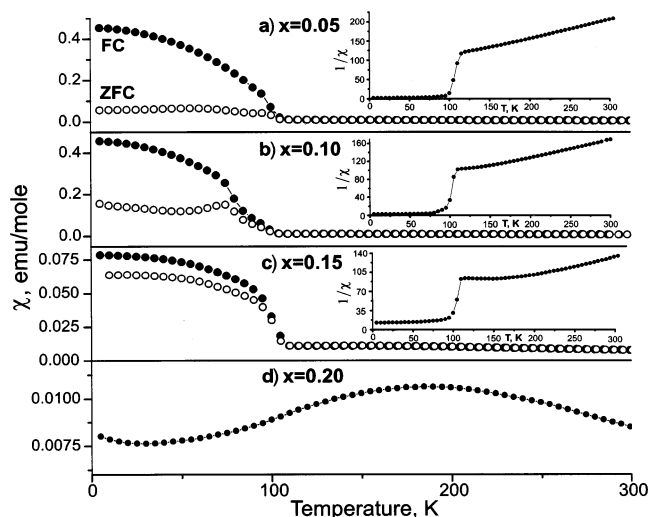(21) Lines, M. E. *J. Phys. Chem. Solids* **1970**, *31*, 101.

Figure 6. Temperature dependence of dc magnetic susceptibility of $Ca_{3-x}Th_xMn_2O_7$ (external field $H = 100$ Oe). Filled and empty circles correspond to field-cooled (FC) and zero-field-cooled (ZFC) data, respectively. Insets show inverse susceptibility; lines are guides to the eye.
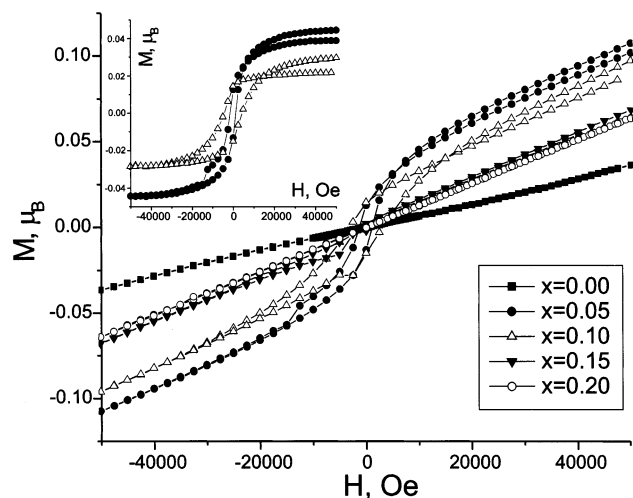

Figure 7. Field dependence of the magnetization of $Ca_{3-x}Th_xMn_2O_7$. Inset: corrected magnetization (after the subtraction of linear AF contribution, see text) for $x = 0.05$ and 0.10 samples. The units are Bohr magnetons per Mn atom.

Once the linear AF contribution has been subtracted (as $\chi_{AF} = \lim_{H \to \infty} \partial M/\partial H$), the corrected magnetization shows clear saturation (Figure 7, inset). The canting angle can thus be estimated as $\tan \theta = M_s/M_0$, where M_s is a uniform saturation magnetization from the (corrected) $M(H)$ curve and M_0 is a staggered magnetization. Since neutron data are unavailable, a theoretical value $M_0 = 3 + x$ was used; thus, the calculated θ represents the lower boundary estimate. The obtained values of θ are $0.8°$ and $0.5°$ for $x = 0.05$ and $x = 0.10$, respectively. For the undoped $Ca_3Mn_2O_7$ the $M(H)$ dependence is nonlinear, suggestive of a field-induced transition at $H \sim 2.5$ T. This prevents precise determination of θ in the above manner. Moreover, the M_s is very small, of the order of 10^{-3} μ_B per Mn atom (which corresponds to $\theta \sim 0.02°$).

The paramagnetic susceptibilities of the $x = 0.1$ and especially $x = 0.15$ samples exhibit significant deviations from a Curie–Weiss (CW) behavior. Attempts to fit the data to a 2D series expansion (similar to that

Table 4. Magnetic Parameters, Room-Temperature Resistivity (ρ_{RT}), and Activation Energy (E_a) for the High-Temperature Resistivity for $Ca_{3-x}Th_xMn_2O_7{}^a$

x	Θ, K	μ_{exp}, μ_B	μ_{th}, μ_B	ρ_{RT}, Ohm·cm	E_a, meV
0.05	−108	4.0	3.93	0.040	47
0.10	−112	4.4	3.98	0.049	56
0.15	−39	4.5	4.03	0.046	67
0.20	−13	4.6	4.08	0.080	-

^{a} μ_{th} is a spin-only theoretical value $2\sqrt{S(S+1)}$. Magnetic parameters for $x = 0.10$ and 0.15 are obtained from the high-temperature Curie–Weiss asymptotics ($T \geq 200$ K).

used for the $Ca_3Mn_2O_7$) failed. Therefore, we suggest that the deviation from CW behavior is not a manifestation of 2D magnetic correlations, but is rather connected with the inhomogeneous magnetic state (see below). The values obtained from CW fits of the data are summarized in Table 4.

A mean-field estimate of J from the value of the Weiss constant (Θ)[22] as

$$k_B\Theta = \frac{2}{3}S(S + 1)(4J_{ab} + J_c) \qquad (5)$$

(there are five nearest neighbors, inter-bilayer coupling is neglected) would obviously depend on the magnetic structure (signs of J_{ab} and J_c). It appears reasonable to assume that the interaction in the ab-plane (J_{ab}) is AF (here and subsequently we use "tetragonal" designations; i.e., c is the stacking axis). Then, from $\Theta = -108$ K for the "G-type" structure (all intra-bilayer nearest neighbor interactions are AF), observed for the stoichiometric $Sr_3Mn_2O_7{}^{23}$ and assuming $J_{ab} = J_c = J$ and $S = 1.525$ ($x = 0.05$), one obtains $J = -8.4$ K. This value is significantly reduced compared with that of undoped $Ca_3Mn_2O_7$ (the value from the location of the 2D maximum of susceptibility is $J = -19.7$ K).

The low magnitude of the FM component (as obtained from low-temperature magnetization) is consistent with DM interaction as its origin. When the values of canting angle, θ, obtained from the low-temperature magnetization, and exchange integral J as above are used, the effective DM coupling constant D can be extracted using the simple relation $\tan \theta = D/|J|$ as $D = 0.12$ and 0.08 K for $x = 0.05$ and $x = 0.10$, respectively. It is approximately 1 order of magnitude smaller than the corresponding value for $LaMnO_3$ (0.7 K).[22]

For the $x = 0.15$ composition χ vs T curve shows similar FM-like upturn. However, the corresponding FM component is roughly 1 order of magnitude smaller than that for $x = 0.1$. For the $x = 0.2$ there is no FM component at all, and the χ vs T curve behaves as for an ordinary AF (Figure 6d). Such behavior suggests a phase separation scenario, reminiscent of that of $Ca_{1-x}Ce_xMnO_3{}^{24}$ and $Sr_{3-x}La_xMn_2O_7;^{25,26}$ that is, we

(22) See for example Prado, F.; Sanchez, R. D.; Caneiro, A.; Causa, M. T.; Tovar, M. *J. Solid State Chem.* **1999**, *146*, 418.

(23) Mitchell, J. F.; Millburn, J. E.; Megarde, M.; Short, S.; Jorgensen, J. D.; Fernandez-Diaz, M. T. *J. Solid State Chem.* **1998**, *141*, 599.

(24) Caspi, E.; Jorgensen, J. D.; Zeng, Z.; Greenblatt, M. Unpublished.

(25) Ling, C. D.; Millburn, J. E.; Mitchell, J. F.; Argyriou, D. N.; Linton, J.; Bordallo, H. N. *Phys. Rev.* **2000**, *B62*, 15096.

(26) Mitchell, J. F.; Ling, C. D.; Millburn, J. E.; Argyriou, D. N.; Berger, A.; Megarde, M. *J. Appl. Phys.* **2001**, *89*, 6618.

(27) Wollan, E. O.; Koehler, W. C. *Phys. Rev.* **1955**, *100*, 545.

propose that the $x = 0.15$ sample is magnetically biphasic with the majority phase being AFM without a FM component (due to a magnetic structure change with possible charge ordering), whereas the minority phase is magnetically identical to lower doping levels (i.e., allows a FM component).

The magnetic properties observed allow us to make definite conclusions about the magnetic structure. It can be shown that for the *Cmcm* symmetry there is only one possible magnetic structure that allows the WFM component. Following ref 13, the existence of WFM is governed by a "parity condition", which states that WFM is possible only for a magnetic structure in which the direction of magnetic moments is the same for all sites, connected by an inversion center or lattice translation. This leaves the G-type structure (in Wollan−Koehler notations;[27] all AF couplings within the bilayer, Figure 4) as the only possibility. Hence, transformation from the G-type structure to any other one would inevitably lead to the disappearance of the FM component (assuming that there would be no crystallographic symmetry change).

Although a detailed neutron diffraction (ND) study is necessary to unambiguously determine the magnetic structure, we tentatively propose the following magnetic structure evolution (Figure 4): from G-type for $Ca_3Mn_2O_7$ to C-type (or C*,[25] which differs by the sign of inter-bilayer coupling only), where AF planes are coupled FM within the bilayer for $x = 0.20$. This kind of transformation (including the intermediate biphasic region) has been directly observed by ND for $Sr_{3-x}La_xMn_2O_7$.[25,26] The indirect evidence for it is the observed reduction of Weiss Θ, reflecting (in this treatment) a positive sign of J_c in eq 5 for a C-type structure.

Such an evolution can be directly suggested from the structural data presented (see above). The perpendicular-to-plane intra-bilayer coupling (the sign of which determines whether G- or C-type structure is realized) is governed by the Mn−O1−Mn bond angle magnitude (ψ). The σ-type AF superexchange interactions weaken with increasing deviation of ψ from the ideal value of 180°, and a G- to C-type transition can be expected for some critical value of ψ. It can also be concluded from the structural data that orthorhombic distortion persists (and even becomes stronger) in the "pure" AF region ($x = 0.20$). Hence, the disappearance of the (weak) FM component at $x = 0.20$ is not a consequence of an orthorhombic-to-tetragonal transition.

Resistivity and Magnetoresistance. As shown in Figure 8, electrical resistivities of the $Ca_3Mn_2O_7$ and doped samples ($x \leq 0.15$) exhibit crossovers (at $T \sim 50-100$ K) from a high-temperature activated region to a low T one, where they can be well-fitted by Mott's law for variable range hopping (VRH):

$$\rho = \rho_0 \exp\left(\frac{T_0}{T}\right)^{\alpha} \left(\alpha = \frac{1}{4}\right) \qquad (6)$$

However, the limited temperature range in this regime prevents unambiguous identification of the conduction type in the low T region (e.g., a nearly identical fit can be obtained using 2D modification of VRH with $\alpha = {}^1/_3$) Nevertheless, the following model can be tentatively proposed. All doped compounds (and $Ca_3Mn_2O_7$, assuming the plausible existence of small

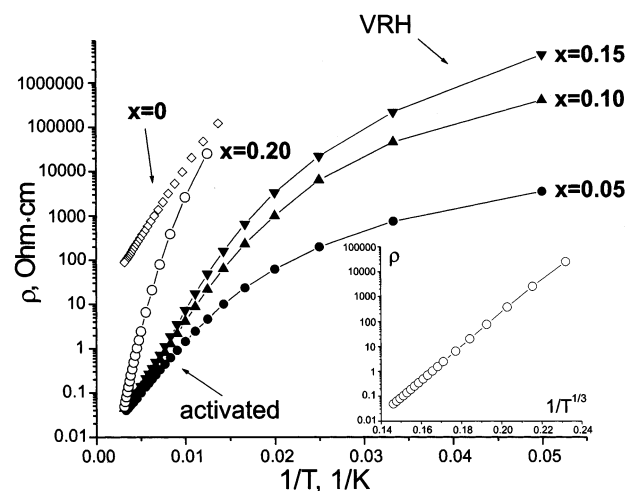**Figure 8.** Temperature dependence of electrical resistivity of $Ca_{3-x}Th_xMn_2O_7$ in Arrhenius coordinates. Inset: $\log(\rho)$ vs $1/T^{1/3}$ (2D VRH coordinates) for $Ca_{2.80}Th_{0.20}Mn_2O_7$. Lines are guides to the eye.

oxygen off-stoichiometry) are characterized by nonintegral band filling. Therefore, true activated conduction (due to a gap in the energy spectrum) is unlikely, and the insulating properties are attributed to strong disorder (Anderson localization). In this treatment the activation energy (E_a) is either related to the "hopping activation energy" in the nearest neighbor hopping (NNH) regime or corresponds to the $E_C - E_F$ difference, where E_F is the Fermi energy and E_C is the mobility edge (high-temperature conduction due to thermal activation to mobility edge). With decreasing temperature the transition to a VRH regime is expected in both cases.[28]

The absolute value of room-temperature resistivities ρ_{RT} and high-temperature E_a are listed in Table 4. ρ_{RT} for all doped samples is approximately 3 orders of magnitude smaller than that for undoped $Ca_3Mn_2O_7$ ($\rho_{RT} \sim 100$ Ohm·cm), consistent with the increased carrier concentration induced by Th substitution. The temperature dependence of the $x = 0.20$ sample can be fitted by a 2D VRH in the entire temperature range (Figure 8, inset). This behavior suggests that the change of the magnetic structure (see above) leads to the confinement of carriers within the perovskite bilayers, and interplane tunneling (supposedly the origin of low-field MR, see below) is hindered.

The $x = 0.05$, 0.10, and 0.15 samples exhibit significant negative magnetoresistance (MR). The maximum MR value is achieved for $x = 0.05$ (MR = −66% at 5 K in an external field $H = 5$ T). Temperature dependence of the MR (in $H = 5$ T) is shown in Figure 9. For higher doping levels MR decreases (for $x = 0.15$ MR = −26% at $H = 5$ T) and completely disappears at $x = 0.20$, remarkably coincident with the disappearance of the FM component in magnetization. The onset of MR for $x = 0.05$ and $x = 0.10$ samples is virtually coincident with the Néel temperature. However, for $x = 0.15$ significant

(28) Mansfield, R. In *Hopping Transport in Solids*; Pollak, M., Shklovskii, B., Eds.; North-Holland: Amsterdam, 1991; Chapter 10.
(29) See for example Hwang, H. Y.; Cheong, S.-W.; Ong, N. P.; Batlogg, B. *Phys. Rev. Lett.* **1996**, *77*, 2041.
(30) Zeng, Z.; Greenblatt, M.; Croft, M. *Phys. Rev.* **2001**, *B63*, 224410.
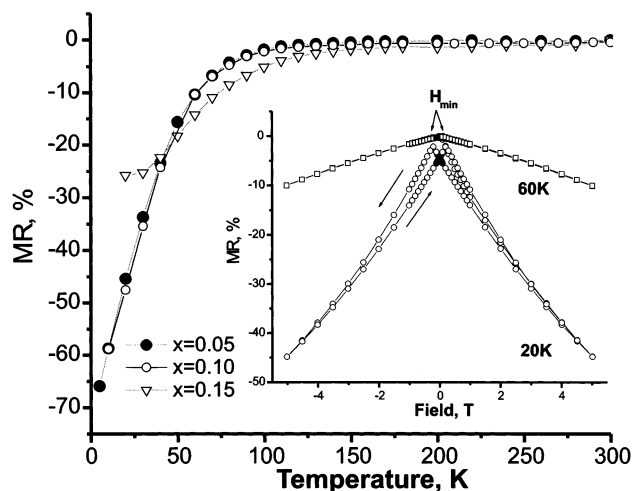
Figure 9. Temperature dependence of MR of $Ca_{3-x}Th_xMn_2O_7$ (x = 0.05, 0.10, and 0.15) in a 5 T field. Inset: Field dependence of MR of $Ca_{2.9}Th_{0.1}Mn_2O_7$ at 20 and 60 K. H_{min} denotes the field at which MR reaches a minimum. Lines are guides to the eye.

MR persists above T_N in the temperature region, characterized by non-CW magnetic susceptibility, supporting the relevance of short-range effects. The field dependence of MR for the x = 0.1 sample for two different temperatures is shown in Figure 9, inset. The temperature dependence of H_{min} (field, corresponding to minimum MR value) parallels the evolution of coercive field H_c, obtained from the magnetization isotherms; however, H_c is approximately twice as small in magnitude ($H_c \sim 1500$ Oe at 20 K). The temperature and field dependence of MR is suggestive of its tunneling origin (either intergrain tunneling, IGT,[29] or interplane tunneling, IPT).[2] The IGT mechanism can be visualized as follows: the (weak) FM component produces the domain structure with domain walls being associated with grain boundaries in the polycrystalline sample.[29] Hence, the field alignment of these domains produces efficient tunneling MR. The IPT MR hypothesis is consistent with the observation of 2D VRH conduction for the x = 0.20 composition (for which MR is absent).

Measurements on a single-crystal sample are necessary to distinguish between those mechanisms.

Conclusions

A new series of Ruddlesden–Popper phases $Ca_{3-x}Th_xMn_2O_7$ has been synthesized by the citrate sol–gel technique. The structural investigation by PXD revealed distortions from the ideal tetragonal (*I4/mmm*) to orthorhombic (*Cmcm* or *Cmc2₁*) symmetry, consistent with magnetic properties and earlier electron diffraction studies of related compounds.

The magnetic properties are suggestive of a certain universality in the behavior of manganites in the electron-doped regime. Th doping induces first a significant FM component (maximum at x = 0.05) in magnetization, which then diminishes with a further increase of x and completely disappears at x_c = 0.2. This behavior parallels the one-electron-doped $Ca_{3-x}La_xMn_2O_7$ series, where x_c = 0.4, which corresponds to the same manganese valence V_{Mn} = +3.8. This overall picture is in turn similar to the one observed for the electron-doped perovskites $Ca_{1-x}Ln_xMnO_3$ (Ln = lanthanide or Th). The x_c value in perovskites is dependent on Ln, that is, tolerance factor value, and for single-electron doping averages to ∼0.15, whereas $x_c \sim 0.08$ (twice as low value) for two-electron-doped systems (Ln = Ce, Th).[7,30]

$Ca_{3-x}Th_xMn_2O_7$ (x = 0.05–0.15) exhibits significant negative magnetoresistance (with maximum MR = −66% at 5 K in an external field H = 5 T for x = 0.05). The temperature and field dependence of MR is suggestive of some kind of tunneling as its origin. A significant MR is found only in those compositions for which a FM component is observed by magnetization measurements.